# A Synthetic Nickel Electrocatalyst with a Turnover Frequency Above 100,000 $s^{-1}$ for $H_2$ Production

Monte L. Helm *et al.*

*Science* **333**, 863 (2011);
DOI: 10.1126/science.1205864



*Science* (print ISSN 0036-8075; online ISSN 1095-9203) is published weekly, except the last week in December, by the American Association for the Advancement of Science, 1200 New York Avenue NW, Washington, DC 20005. 

way) was measured (*24*) and was <0.1%. Moreover, in the case of externally induced strain, the direction of mechanical deformations would be related to the contact geometry, not to the crystallographic orientation, and would vary from sample to sample. Instead, we find the same feature in four different devices, which would require a rather narrow range of parameters (size and orientation of the principal axes of strain tensor) to be repeated precisely in different samples. We also have considered whether our results can be explained in terms of a spontaneous gap opening in the bilayer spectrum (*35*). In this case, the transport at the neutrality point (with or without magnetic field) would be dominated by a network of one-dimensional channels between the domains of gaps with alternating signs. This would result in a minimum conductivity value that depends strongly on the strain prehistory, in contrast to values reproducibly observed in our experiments. Also, this model would not likely produce a drop in the resistance at $\nu = 0$, as observed in our experiments. These differences suggest that the observed reconstruction of the spectrum is the result of an intrinsic modification of the electronic system; in particular, it can be caused by the recently predicted "nematic" phase transition (*9*, *10*) in bilayer graphene.

**References and Notes**


1. K. S. Novoselov *et al.*, *Science* **306**, 666 (2004).
2. A. K. Geim, K. S. Novoselov, *Nat. Mater.* **6**, 183 (2007).
3. A. H. Castro Neto, F. Guinea, N. M. R. Peres, K. S. Novoselov, A. K. Geim, *Rev. Mod. Phys.* **81**, 109 (2009).
4. K. S. Novoselov *et al.*, *Nat. Phys.* **2**, 177 (2006).
5. E. McCann, V. I. Fal'ko, *Phys. Rev. Lett.* **96**, 086805 (2006).
6. E. V. Castro, N. M. R. Peres, T. Stauber, N. A. P. Silva, *Phys. Rev. Lett.* **100**, 186803 (2008).
7. R. Nandkishore, L. Levitov, *Phys. Rev. Lett.* **104**, 156803 (2010).
8. F. Zhang, H. Min, M. Polini, A. H. MacDonald, *Phys. Rev. B* **81**, 041402 (2010).
9. Y. Lemonik, I. L. Aleiner, C. Toke, V. I. Fal'ko, *Phys. Rev. B* **82**, 201408 (2010).
10. O. Vafek, K. Yang, *Phys. Rev. B* **81**, 041401 (2010).
11. V. Oganesyan, S. A. Kivelson, E. Fradkin, *Phys. Rev. B* **64**, 195109 (2001).
12. E. Fradkin, S. A. Kivelson, V. Oganesyan, *Science* **315**, 196 (2007).
13. E. Fradkin, S. A. Kivelson, M. J. Lawler, J. P. Eisenstein, A. P. Mackenzie, *Annu. Rev. Condens. Matter Phys.* **1**, 153 (2010).
14. M. P. Lilly, K. B. Cooper, J. P. Eisenstein, L. N. Pfeiffer, K. W. West, *Phys. Rev. Lett.* **82**, 394 (1999).
15. M. P. Lilly, K. B. Cooper, J. P. Eisenstein, L. N. Pfeiffer, K. W. West, *Phys. Rev. Lett.* **83**, 824 (1999).
16. R. R. Du *et al.*, *Solid State Commun.* **109**, 389 (1999).
17. Y. Ando, K. Segawa, S. Komiya, A. N. Lavrov, *Phys. Rev. Lett.* **88**, 137005 (2002).
18. V. Hinkov *et al.*, *Science* **319**, 597 (2008).
19. T. M. Chuang *et al.*, *Science* **327**, 181 (2010).
20. R. A. Borzi *et al.*, *Science* **315**, 214 (2007).
21. X. Du, I. Skachko, A. Barker, E. Y. Andrei, *Nat. Nanotechnol.* **3**, 491 (2008).
22. K. I. Bolotin *et al.*, *Solid State Commun.* **146**, 351 (2008).
23. B. E. Feldman, J. Martin, A. Yacoby, *Nat. Phys.* **5**, 889 (2009).
24. E. V. Castro *et al.*, *Phys. Rev. Lett.* **105**, 266601 (2010).
25. L. A. Ponomarenko *et al.*, *Phys. Rev. Lett.* **102**, 206603 (2009).
26. See supporting material on *Science* Online.
27. M. I. Katsnelson, *Eur. Phys. J. B* **51**, 157 (2006).
28. I. Snyman, C. W. J. Beenakker, *Phys. Rev. B* **75**, 045322 (2007).
29. J. Cserti, A. Csordás, G. Dávid, *Phys. Rev. Lett.* **99**, 066802 (2007).
30. I. M. Lifshitz, *Sov. Phys. JETP* **11**, 1130 (1960).
31. R. T. Weitz, M. T. Allen, B. E. Feldman, J. Martin, A. Yacoby, *Science* **330**, 812 (2010).
32. E. V. Castro *et al.*, *Phys. Rev. Lett.* **99**, 216802 (2007).
33. M. Mucha-Kruczyński, I. L. Aleiner, V. I. Fal'ko, *Phys. Rev. B* **84**, 041404 (2011).
34. Y.-W. Son, S.-M. Choi, Y. P. Hong, S. Woo, S.-H. Jhi, http://arxiv.org/abs/1012.0643v1 (2010).
35. R. Nandkishore, L. Levitov, *Phys. Rev. B* **82**, 115124 (2010).


**Acknowledgments:** This research was supported by the European Research Council, European Commision FP7, Engineering and Physical Research Council (UK), the Royal Society, U.S. Office of Naval Research, U.S. Air Force Office of Scientific Research, and the Körber Foundation.

**Supporting Online Material**

www.sciencemag.org/cgi/content/full/333/6044/860/DC1
SOM Text
Figs. S1 to S3

20 May 2011; accepted 29 June 2011
10.1126/science.1208683

# A Synthetic Nickel Electrocatalyst with a Turnover Frequency Above 100,000 $s^{-1}$ for $H_2$ Production

**Monte L. Helm,[1,2]* Michael P. Stewart,[1] R. Morris Bullock,[1]† M. Rakowski DuBois,[1] Daniel L. DuBois[1]†**

**Reduction of acids to molecular hydrogen as a means of storing energy is catalyzed by platinum, but its low abundance and high cost are problematic. Precisely controlled delivery of protons is critical in hydrogenase enzymes in nature that catalyze hydrogen ($H_2$) production using earth-abundant metals (iron and nickel). Here, we report that a synthetic nickel complex, $[Ni(P^{Ph}_2N^{Ph})_2](BF_4)_2$, ($P^{Ph}_2N^{Ph}$ = 1,3,6-triphenyl-1-aza-3,6-diphosphacycloheptane), catalyzes the production of $H_2$ using protonated dimethylformamide as the proton source, with turnover frequencies of 33,000 per second ($s^{-1}$) in dry acetonitrile and 106,000 $s^{-1}$ in the presence of 1.2 M of water, at a potential of −1.13 volt (versus the ferrocenium/ferrocene couple). The mechanistic implications of these remarkably fast catalysts point to a key role of pendant amines that function as proton relays.**

Electrocatalysts that efficiently convert the energy from electricity into chemical bonds in fuels (such as hydrogen), or the reverse, converting chemical energy to electrical energy, will play a vital role in future energy storage and energy delivery systems. Hydrogenase enzymes (*1*, *2*) efficiently catalyze both the production and the oxidation of hydrogen using earth-abundant metals (nickel and iron). Detailed information about catalytic reactions of enzymes has been obtained from protein film voltammetry (*3*), but enzymes are difficult to obtain in sufficient amounts to adapt for commercial applications, and their stability is often limited outside of their native environment (*4*). Platinum is an excellent catalyst for hydrogen oxidation and production, but the scarcity and high cost of precious metals pose serious limitations to widespread use. These considerations have led to efforts to design molecular catalysts that employ earth-abundant metals. Synthetic complexes of nickel (*5*–*8*), cobalt (*9*–*12*), iron (*13*–*15*), or molybdenum (*16*, *17*) have been developed recently as electrocatalysts for the production of hydrogen.

In nature, [FeFe] hydrogenase enzymes catalyze the formation of $H_2$ from water, with reported rate constants as high as 9000 $s^{-1}$ at 30°C (*18*). Crystallographic and spectroscopic studies have led to the proposal of the structure of the active site of the [FeFe] hydrogenase enzyme shown in structure **1** of Fig. 1 (*1*). The amine base positioned near the iron center has been proposed to function as a proton relay that facilitates the formation or cleavage of the H-H bond. Substantial progress on the preparation of structural mimics of the active site (*13*, *14*, *19*) provides insight into mechanistic features of the catalytic reaction. For example, Rauchfuss and co-workers have recently demonstrated that a pendant amine in a structural model closely related to **1** plays a key role in the production of $H_2$ (*20*). Efforts in our laboratory have focused on developing mononuclear complexes of Fe, Co, and Ni that contain an amine base in the second coordination sphere, adjacent to a vacant coordination site or a hydride ligand on the metal center (*21*–*23*). Some of these complexes are very effective electrocatalysts for $H_2$ formation or $H_2$ oxidation,

[1]Center for Molecular Electrocatalysis, Chemical and Materials Sciences Division, Pacific Northwest National Laboratory, Post Office Box 999, K2-57, Richland, WA 99352, USA. [2]Chemistry Department, Fort Lewis College, 1000 Rim Drive, Durango, CO 81301, USA.

*Sabbatical visitor at Pacific Northwest National Laboratory, 2010–2011.

†To whom correspondence should be addressed. E-mail: morris.bullock@pnnl.gov (R.M.B.); daniel.dubois@pnnl.gov (D.L.D.)

and they provide functional models for the proton relay functions of the hydrogenase enzymes. For example, a series of $[Ni(P^{Ph}_2N^{C_6H_4X}_2)_2]^{2+}$ catalysts with structure **2** have been studied. Under optimized conditions, $[Ni(P^{Ph}_2N^{C_6H_4Br}_2)_2]^{2+}$, with bromophenyl substituents on the amine ligand, catalyzed the formation of $H_2$ with turnover frequencies as high as 1040 $s^{-1}$ and an overpotential of ~290 mV (*7*).

Mechanistic (*5*, *7*) and theoretical (*24*) studies of the $[Ni(P^{R}_2N^{R'}_2)_2]^{2+}$ catalysts suggest that the transition state for $H_2$ production has structure **3** shown in Fig. 1, in which the formation of the H-H bond occurs in a heterolytic manner, with the pendant amine acting as a proton donor and the nickel functioning as a hydride donor. The formation of transition state **3** involves the reduction of the starting complex **2** by two electrons and the addition of two protons. Previous nuclear magnetic resonance spectroscopic studies on reduction and protonation of closely related analogs of **2** have shown that intermediates formed before transition state **3** are isomeric Ni(0) complexes in which an amine in each ligand is protonated. The double protonation reaction of $Ni^0(P^{Ph}_2N^{Bn}_2)_2$ (where Bn is benzyl) forms structure **4** as the kinetic product (Fig. 2) (*25*). The kinetic product isomerizes to form an equilibrium mixture of structures **4**, **5,** and **6** by an intermolecular process that involves deprotonation by a base in solution and reprotonation at an endo position. This process is assisted by water. Only isomer **6** can readily convert to transition state **3** by a simple intramolecular proton transfer from nitrogen to nickel, and therefore only isomer **6** is active in the catalytic cycle. These studies led us to propose that only a fraction of the doubly protonated Ni(0) intermediates formed during hydrogen production are in the catalytically active form, isomer **6**, and that significantly higher catalytic rates might be achieved if the stabilized exo-protonated structures could be avoided. We also proposed that the observed enhancement of turnover frequencies by water is a result of its role in converting the exo-protonated isomers **4** and **5** to the endo-endo isomer **6** (*7*).

Here, we report the synthesis of $[Ni(P^{Ph}_2N^{Ph})_2](BF_4)_2$, **7**, which was isolated as orange crystals in 75% yield from the reaction shown in Scheme 1 (*26*). The new complex contains two seven-membered cyclic diphosphine ligands, $P^{Ph}_2N^{Ph}$ (where $P^{Ph}_2N^{Ph}$ = 1,3,6-triphenyl-1-aza-3,6-diphosphacycloheptane). Because this ligand has just one pendant amine, it precludes the possibility of forming nonproductive pinched isomers analogous to **4** and **5** upon reduction and protonation of **7**. Although the reduced form of **7** can be protonated either endo or exo with respect to Ni, stabilization by a second N•••H interaction in an exo-exo form (e.g., as in **4**) is not possible. The molecular structure of **7** determined by x-ray diffraction (Fig. 3) is a distorted square planar complex with all four Ni-P bond distances nearly equal at 2.21 to 2.22 Å. Complexation of both phosphorus atoms in each $P^{Ph}_2N^{Ph}$ ligand in **7** forms one five-membered chelate ring and a six-membered ring that incorporates the pendant amine. In contrast, both of the eight-membered cyclic ligands in **2** form two six-membered chelate rings upon binding to the metal. As a result, the P-Ni-P bond angle (79.83°) for each of the two diphosphine ligands in **7** is smaller than the 82° to 84° typically observed for the P-Ni-P bonds in derivatives of **2** (*5*, *7*). This smaller bite angle leads to a decrease in the steric interactions between the phenyl substituents on adjacent phosphorus atoms of the two ligands in **7**. As a result, **7** is much more planar than the corresponding derivatives of **2**. For $[Ni(P^{Ph}_2N^{C_6H_4Me}_2)_2]^{2+}$, the dihedral angle between the two planes defined by the Ni atom and the two phosphorus atoms of each diphosphine ligand is 24.16° (*7*), whereas for **7,** it is 0.0°. Thus, the replacement of two eight-membered cyclic ligands with two seven-membered cyclic ligands in these nickel complexes has significant structural consequences.

The cyclic voltammogram of an acetonitrile solution of $[Ni(P^{Ph}_2N^{Ph})_2]^{2+}$, **7**, shows one reversible reduction wave assigned to overlapping Ni(II/I)/Ni(I/0) couples at –1.13 V versus the ferrocenium/ferrocene couple (simulated as two one-electron waves at –1.09 and –1.16 V). (See Supporting Online Material for a cyclic voltammogram of **7**, fig. S3, and a detailed analysis.) Figure 4 shows successive cyclic voltammograms of **7** recorded in acetonitrile with increasing concentrations of protonated dimethylformamide {[(DMF)H]OTf, $pK_a$ = 6.1 in acetonitrile} (*27*). A catalytic wave for the reduction of protons is observed with a half-wave potential of –1.13 V in the presence of 0.20 M acid, corresponding to an overpotential of ~625 mV determined using the method of Evans (*28*). The catalytic production of $H_2$ was confirmed by a gas chromatographic analysis of the gas produced during a controlled potential electrolysis experiment (–1.4 V, current efficiency 99 ± 5% for $H_2$ production, 11 turnovers with no observable decomposition). At high acid concentrations relative to the catalyst, Eq. 1 can be used to calculate pseudo first-order rate constants, $k_{obs}$, for $H_2$ evolution.

$$\frac{i_{cat}}{i_p} = \frac{2}{0.446}\sqrt{\frac{RTk_{obs}}{F\upsilon}} \qquad (1)$$

In this equation, $i_{cat}$ is the catalytic current, $i_p$ is the peak current measured in the absence of acid, 2 is the number of electrons involved in the catalytic reaction, $k_{obs}$ is the observed first-order rate constant, $R$ is the universal gas constant, $T$ is the temperature in Kelvin, $F$ is Faraday's constant, υ is the scan rate, and 0.446 is a constant determined by numerical solution of the diffusion equations (*29*). The value of $k_{obs}$ increases linearly with acid concentration (fig. S9), indicating a first-order dependence of the catalytic rate on acid concentration. At the highest acid concentration studied (0.43 M), a value of $i_{cat}/i_p$ = 38 was measured, corresponding to a turnover frequency of 33,000 $s^{-1}$ at 22°C.

At 0.43 M [(DMF)H]OTf, cyclic voltammetry and ultraviolet-visible absorption spectra indicated that less than 5% decomposition of the catalyst occurred over the 0.5 hours required for the catalytic studies. However, higher acid concentrations could not be used to determine reliable turnover frequencies because of catalyst decomposition under more strongly acidic conditions. The catalyst is stable in the presence of

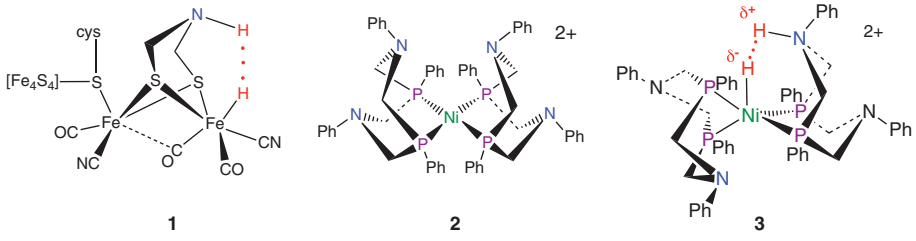


**Fig. 1.** Proposed structure of the [FeFe] hydrogenase active site (**1**) based on crystallographic data (*1*); synthetic Ni complex (**2**) that catalyzes $H_2$ formation, with pendant amines that function as proton relays (*7*); proposed transition state (*24*) (**3**) for production of hydrogen catalyzed by **2**.

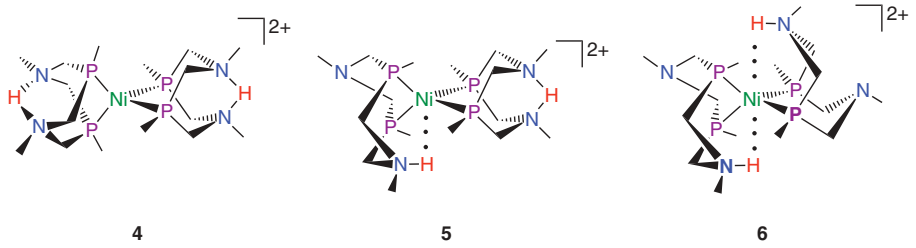


**Fig. 2.** Doubly protonated Ni(0) intermediates (isomers **4**, **5**, and **6**) involved in the production of $H_2$ catalyzed by **2**. For clarity, organic substituents on the N and P are not shown.

$H_2O$, and the addition of $H_2O$ (1.2 M) to the mixture results in a further enhancement of the catalytic current beyond the maximum $i_{cat}$ achieved with acid alone, resulting in a value of $i_{cat}/i_p$ = 74, corresponding to a turnover frequency of 106,000 $s^{-1}$. Simulations of the voltammograms obtained under catalytic conditions are in agreement with the experimentally measured $i_{cat}/i_p$ = 74 (fig. S10 and table S3). The additional rate enhancement in the presence of water is attributed to the ability of water to enhance the rate of conversion of exo to endo isomers.

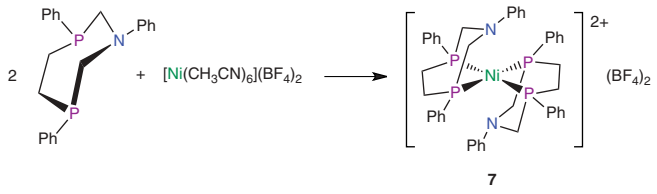


**Scheme 1.**

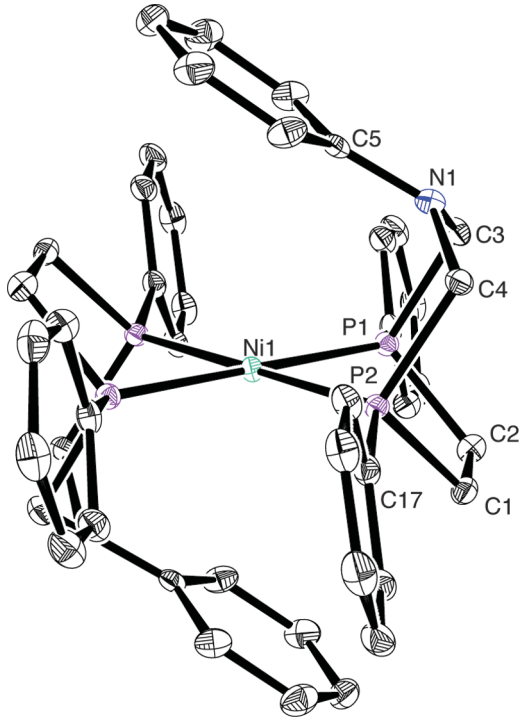


**Fig. 3.** Solid-state molecular structure of $[Ni(P^{Ph}_2N^{Ph})_2](BF_4)_2{\cdot}2CH_3CN$, **7**. The $BF_4^-$ counterions, $CH_3CN$ solvent molecules, and H atoms have been omitted for clarity. Thermal ellipsoids are shown at the 50% probability level.

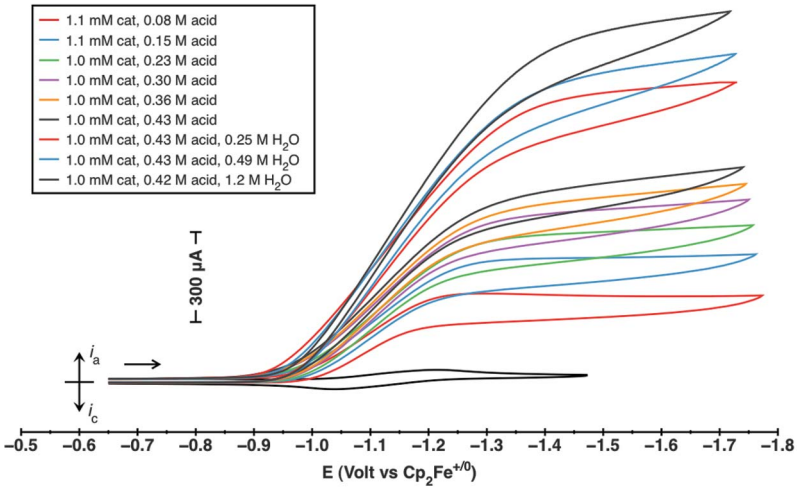


**Fig. 4.** Successive cyclic voltammograms of 1.0 mM **7** in $CH_3CN$ (0.10 M $[Bu_4N][PF_6]$) at increasing concentrations of [(DMF)H]OTf, followed by addition of small aliquots of $H_2O$. Conditions: 1 mm glassy-carbon working electrode; 22°C; scan rate 10 V/s.

The turnover frequencies measured for **7** substantially exceed the highest turnover frequency reported for the formation of $H_2$ catalyzed by the [FeFe] hydrogenase enzyme, 9000 $s^{-1}$ at 30°C (*18*). This comparison, however, must be tempered by the recognition that the overpotential of the natural hydrogenase is thought to be less than 100 mV, significantly lower than the overpotential for **7**. The exceptionally high turnover frequency observed for **7** is about two orders of magnitude larger than that observed for **2** under comparable conditions (590 $s^{-1}$ with an overpotential of 300 mV, increasing to 720 $s^{-1}$ when water is added) (*7*). Most important, our results clearly indicate that properly designed pendant amine bases in the second coordination sphere that function as proton relays are capable of promoting extremely fast H-H bond formation and proton transfer from solution to the metal center.

The observed first-order dependence on acid is consistent with a one- or two-electron reduction of **7**, followed by rate-determining protonation of the reduced complex. In contrast, **2** exhibits catalytic rates that are second-order in acid at concentrations below ~0.1 M and independent of acid above ~0.2 M concentrations (*7*). Although the overall catalytic mechanisms for **2** and **7** are likely quite similar, changing the rate-determining step has significant effects on the observed catalytic rates. For derivatives of **2**, the overall catalytic rate is predominantly controlled by two factors, the formation of endo-endo isomers such as **6** and $H_2$ elimination via transition state **3**. For **7**, the endo-protonation of a reduced intermediate is the rate-determining event. This implies that the rate of $H_2$ elimination via transition state **3** must be faster for **7** than for **2**. This is likely the result of a more hydridic Ni-H bond for **7**, which has been shown to correlate with more negative Ni(II/I) reduction potentials in these $[Ni(diphosphine)_2]^{2+}$ complexes (*30*). The more negative Ni(II/I) potential for **7** (–1.13 V) compared with that of **2** (–0.84 V) is expected on the basis of their structural differences (greater planarity of **7**), and this modification contributes to the significantly larger overpotential for $H_2$ production observed for **7**.

In conclusion, the observation of an extremely high turnover frequency for **7** clearly demonstrates that its positioned proton relays support high rates for all of the individual catalytic steps, that is, inter- and intramolecular proton transfer, electron transfer (or proton-coupled electron transfer steps), and heterolytic formation of $H_2$. These results highlight the substantial promise that designed molecular catalysts hold for the electrocatalytic production of hydrogen. The high sensitivity of catalytic rates to the incorporation and arrangement of pendant amines in the ligand suggests a potentially broader role that proton relays may play in other important multi-proton, multi-electron catalytic reactions, such as the reduction of oxygen and oxidation of water.

**References and Notes**

1. J. C. Fontecilla-Camps, A. Volbeda, C. Cavazza, Y. Nicolet, *Chem. Rev.* **107**, 4273 (2007).
2. P. M. Vignais, B. Billoud, *Chem. Rev.* **107**, 4206 (2007).
3. K. A. Vincent, A. Parkin, F. A. Armstrong, *Chem. Rev.* **107**, 4366 (2007).
4. J. A. Cracknell, K. A. Vincent, F. A. Armstrong, *Chem. Rev.* **108**, 2439 (2008).
5. A. D. Wilson *et al.*, *J. Am. Chem. Soc.* **128**, 358 (2006).
6. A. D. Wilson *et al.*, *Proc. Natl. Acad. Sci. U.S.A.* **104**, 6951 (2007).
7. U. J. Kilgore *et al.*, *J. Am. Chem. Soc.* **133**, 5861 (2011).
8. A. Le Goff *et al.*, *Science* **326**, 1384 (2009).
9. X. Hu, B. S. Brunschwig, J. C. Peters, *J. Am. Chem. Soc.* **129**, 8988 (2007).
10. P.-A. Jacques, V. Artero, J. Pécaut, M. Fontecave, *Proc. Natl. Acad. Sci. U.S.A.* **106**, 20627 (2009).
11. V. Artero, M. Fontecave, *Coord. Chem. Rev.* **249**, 1518 (2005).
12. J. L. Dempsey, B. S. Brunschwig, J. R. Winkler, H. B. Gray, *Acc. Chem. Res.* **42**, 1995 (2009).
13. T. Liu, M. Y. Darensbourg, *J. Am. Chem. Soc.* **129**, 7008 (2007).
14. F. Gloaguen, T. B. Rauchfuss, *Chem. Soc. Rev.* **38**, 100 (2009).
15. S. Kaur-Ghumaan, L. Schwartz, R. Lomoth, M. Stein, S. Ott, *Angew. Chem. Int. Ed.* **49**, 8033 (2010).
16. A. M. Appel, D. L. DuBois, M. R. DuBois, *J. Am. Chem. Soc.* **127**, 12717 (2005).
17. H. I. Karunadasa, C. J. Chang, J. R. Long, *Nature* **464**, 1329 (2010).
18. M. Frey, *ChemBioChem* **3**, 153 (2002).
19. C. Tard *et al.*, *Nature* **433**, 610 (2005).
20. B. E. Barton, M. T. Olsen, T. B. Rauchfuss, *J. Am. Chem. Soc.* **130**, 16834 (2008).
21. C. J. Curtis *et al.*, *Inorg. Chem.* **42**, 216 (2003).
22. M. Rakowski DuBois, D. L. DuBois, *Acc. Chem. Res.* **42**, 1974 (2009).
23. D. L. DuBois, R. M. Bullock, *Eur. J. Inorg. Chem.* **2011**, 1017 (2011).
24. M. Dupuis, S. Chen, S. Raugei, D. L. DuBois, R. M. Bullock, *J. Phys. Chem. A* **115**, 4861 (2011).
25. A. M. Appel *et al.*, *ACS Catalysis* **1**, 777 (2011).
26. Materials and methods and spectroscopic data are available as supporting material on *Science* Online.
27. K. Izutsu, *Acid-Base Dissociation Constants in Dipolar Aprotic Solvents* (Blackwell Scientific Publications, Oxford, 1990).
28. G. A. N. Felton, R. S. Glass, D. L. Lichtenberger, D. H. Evans, *Inorg. Chem.* **45**, 9181 (2006).
29. A. J. Bard, L. R. Faulkner, *Electrochemical Methods: Fundamentals and Applications* (Wiley, New York, ed. 2, 2001).
30. D. E. Berning *et al.*, *Organometallics* **20**, 1832 (2001).



**Acknowledgments:** This research was supported as part of the Center for Molecular Electrocatalysis, an Energy Frontier Research Center funded by the U.S. Department of Energy, Office of Science, Office of Basic Energy Sciences. Pacific Northwest National Laboratory is operated by Battelle for the U.S. Department of Energy. Structural parameters for **4** are available free of charge from the Cambridge Crystallographic Data Centre under CCDC 828010. We thank J. A. S. Roberts for help with the simulations of the cyclic voltammograms.


**Supporting Online Material**

www.sciencemag.org/cgi/content/full/333/6044/863/DC1
Materials and Methods
SOM Text
Figs. S1 to S11
Tables S1 to S4
References (*31*–*33*)


21 March 2011; accepted 28 June 2011
10.1126/science.1205864


# The Persistently Variable "Background" Stratospheric Aerosol Layer and Global Climate Change


**S. Solomon,[1,2]* J. S. Daniel,[1] R. R. Neely III,[1,2,5,6] J.-P. Vernier,[3,4] E. G. Dutton,[5] L. W. Thomason[3]**



**Recent measurements demonstrate that the "background" stratospheric aerosol layer is persistently variable rather than constant, even in the absence of major volcanic eruptions. Several independent data sets show that stratospheric aerosols have increased in abundance since 2000. Near-global satellite aerosol data imply a negative radiative forcing due to stratospheric aerosol changes over this period of about −0.1 watt per square meter, reducing the recent global warming that would otherwise have occurred. Observations from earlier periods are limited but suggest an additional negative radiative forcing of about −0.1 watt per square meter from 1960 to 1990. Climate model projections neglecting these changes would continue to overestimate the radiative forcing and global warming in coming decades if these aerosols remain present at current values or increase.**


Understanding climate changes on time scales of years, decades, centuries, or more requires determining the effects of all external drivers of radiative forcing of Earth's climate, including anthropogenic greenhouse gases and aerosols, natural aerosols, and solar forcing, as well as natural internal variability. Much debate has focused on whether the rate of global warming of the past decade or so is consistent with global climate model estimates (*1*), requiring careful examination of all radiative forcing terms. Most of the global warming of the past half-century has been driven by continuing increases in anthropogenic greenhouse gases (*2*), but natural aerosols from particular "colossal" volcanic eruptions [see the index of volcanic activity definitions in (*3*)] have significantly cooled the global climate at times, including, for example, the "year without a summer" experienced after the eruption of the Tambora volcano in 1815 and notable cooling after the Pinatubo eruption in 1991 (*4*, *5*). As used here, "colossal" or "major" refers to specific volcanic eruptions that have been generally recognized not only as extremely large but also as having injected a great deal of gaseous sulfur directly into the tropical stratosphere. Tropical eruptions are thought to be especially important for climate change because the injected material can be transported into the stratospheres of both hemispheres and affect the entire globe for many months.

The cooling effect of volcanic eruptions mainly arises not from the injected ash but from $SO_2$ injected by plumes that are able to reach beyond the tropical tropopause into the stratosphere, whereupon the $SO_2$ oxidizes and temporarily increases the burden of stratospheric particles. Stratospheric aerosols are composed largely of dilute sulfuric acid droplets that effectively reflect some incoming solar energy back to space. The radiative cooling due to increases in these particles is linked to the associated optical depth increases. Observations show that the volcanic particles from the colossal eruptions of El Chichón and Pinatubo in 1982 and 1991, respectively, decayed from the stratosphere with e-folding times (the time interval in which an exponentially decaying quantity decreases by a factor of $e$) of about a year (*5*).

Early measurements of the stratospheric aerosol layer around 1960 by Junge *et al.* (*6*) were carried out at a time when no colossal eruptions had occurred in many years. These data are subject to large instrumental uncertainty, but suggested an apparent "background" stratospheric aerosol layer, with aerosol burdens too small to measurably influence the global climate system. Crutzen (*7*) proposed that the dominant source of the background stratospheric aerosol layer was carbonyl sulfide (OCS), because other sulfur sources were thought to be too reactive or too soluble in rainwater to reach the stratosphere in significant amounts. But observations of the amount of background stratospheric aerosol since at least the 1970s using improved instrumentation reveal abundances that are far too large to be due mainly to OCS (*8*). Some studies have suggested that an important source of the background stratospheric aerosol layer may be anthropogenic sulfur ($SO_2$ from coal burning, biomass burning, etc.) that can be transported


[1]Chemical Sciences Division, National Oceanic and Atmospheric Administration (NOAA), Earth System Research Laboratory, Boulder, CO 80305, USA. [2]Department of Atmospheric and Oceanic Sciences, University of Colorado, Boulder, CO 80305, USA. [3]NASA Langley Research Centre, Hampton, VA, USA. [4]Laboratoire Atmosphères, Milieux, Observations Spatiales, CNRS–Institut National des Sciences de l'Univers, Université de Versailles St Quentin, Université de Paris 6, France. [5]Global Monitoring Division, NOAA, Earth System Research Laboratory, Boulder, CO, USA. [6]Cooperative Institute for Research in Environmental Science, University of Colorado, Boulder, CO, USA.

*To whom correspondence should be addressed. E-mail: susan.solomon@colorado.edu